IIETA International Information and Engineering Technology Association
Advancing the World of Information and Engineering

Traitement du Signal
Vol. 39, No. 3, June, 2022, pp. 879-892
Journal homepage: http://iieta.org/journals/ts

Non-Local Retinex Based Dehazing and Low Light Enhancement of Images

Hari Unnikrishnan*, Ruhan Bevi Azad

SRM Institute of Science and Technology, Chennai 603203, India

Corresponding Author Email: hu8555@srmist.edu.in

https://doi.org/10.18280/ts.390313

Received: 11 April 2022
Accepted: 20 May 2022

Keywords:
image dehazing, dark channel prior, non-local retinex, low light image, guided filter

ABSTRACT

We know that a vast amount of research has recently been done on dehazing single images. More work is done on day-time images than night-time images. Also, enhancement of low light images is another area in which lots of research going on. In this paper, a simple yet effective unified variational model is proposed for dehazing of day and night images and low-light enhancement based on non-local global variational regularization. Given the relation between image dehazing and retinex, the haze removal process can minimize a variational retinex model. Estimating of ambient light and transmission maps is a key step in modern dehazing methods. Atmospheric light is not uniform and constant for hazy night images, as night scenes often contain multiple light sources. Often lit and non-illuminated regions have different colour characteristics and cause total variation colour distortion and halo artifacts. Our work directly implements a non-local retinal model based on the L2 norm that simulates the average activity of inhibitory and excitatory neuronal populations in the cortex to overcome this problem. This potential biological feasibility of the L2 norm of our work is divided into two parts using a filtered gradient approach, the reflection sparse prior and the reflection gradient fidelity before the observed image gradient. This unified framework of NLTV-Retinex and DCP efficiently performs low-light enhancement and dehazing of day and night images. We show results obtained using our method on daytime and night-time images and a low-light image dataset. We quantitatively and qualitatively compare our results with recently reported methods, which demonstrate the effectiveness of our method.

1. INTRODUCTION

During the past decade, a lot of research has enhanced the quality of hazy or foggy images. In computer vision applications for outdoor environments, the visibility and contrast of images captured in foggy weather are rigorously reduced [1-3]. Since photo quality is mainly affected by the existence of small dust particles in the air which scatter the original light reflected by object in the scene before absorbed by sensor, this leads to poor contrast quality and the depth details lost. Image dehazing is desirable in feature extraction applications such as digital video surveillance, aerial survey, and driverless car, thereby enhancing the scene visibility and appropriate correction in the color shift.

Haze occurs due to the scattering of light through the microscopic water droplets. The Number of pixels in a frame can be enhanced by removal of noise in video. Noise present degrades per pixel image hence lessening robustness and efficiency. The proposed work deals with removal of haze from noisy atmospheric images. It helps to overcome the problem of haze and poor visibility. This reduces trade-off between contrast and saturation of images, thus preserving the quality of the recovered image.

The method used enhances the quality of an image by removing atmospheric noise like haze and fog and performs effective denoising of images considering Retinex properties such as illumination and reflectance components of images. The algorithm used in denoising atmospheric images is Dark Channel Prior Algorithm. It first computes the parameters such as airlight estimate and rough depth of the scene. There are various techniques based on DCP are discussed. They found solutions simply by using the single input hazy image. Even though these techniques are very effective and have been widely used on hazy daylight scenes, they perform poorly with restrictions on hazy night-time scenes. Since, several light-emitting objects causes a non-uniform brightness, haze removal from images captured at night becomes intricate. So only a limited number of researches have been carried out on the night-time haze elimination issues.

The main research aim is to enhance the low-light night-time hazy scenes. To achieve this goal, a novel method which combines DCP and non-local retinex algorithms is developed to achieve contrast enhancement and preserve edges. Experimental results of the proposed system on LoL database images provide promising results in terms of Peak Signal-to-Noise Ratio (PSNR), Structural Similarity Index Measure (SSIM). The proposed system achieves ~15% more PSNR, 20% more SSIM than Ancutis algorithm and also it outperforms other existing algorithms in section 2 in evaluating the LoL image dataset.

The organization of the paper is as follows: Section 2 reviews the current literature on low-light image enhancement. The proposed system is discussed in section 3 with the help of haze image-atmospheric scattering model, estimation of dark channel and atmospheric light, non-local retinex, transmission optimization, and scene radiance recovery. Section 4 discusses the experimental results of the proposed system on LoL database images and evaluated in terms of PSNR and SSIM.

The conclusions are provided in the last section.

2. RELATED WORK

In past few years, there is plenty of research works carried out with enormous progress to improve the visibility of hazy images. In the domain research of improving the contrast and clarity of hazy images, various methods like dark channel prior, color attenuation prior, fusion-based dehazing, histogram equalization, wavelet method and retinex method.

Narasimhan and Nayar [4] proposed that scene radiance the structure can be recovered from the hazy scene using multiple images and spatial information. In literature, plenty of prior based methods for dehazing of single images. Dark channel prior [1-5] is one of the popular priorities, improving the quality of hazy images with poor visibility. Pal [6] compared the DCP on real-time, and the experimental foggy image quality improved, but the time taken to process successive frames was longer. Berman et al. [7] proposed an algorithm for dehazing using haze lines to estimate atmospheric light. The color attenuation prior [8] is presented, and this algorithm thereby efficiently restores the degraded hazy images. Learning-based dehazing is discussed by Cai et al. [9] for end-to-end haze removal process. Wang et al. [10] proposed dark channel prior based single image dehazing with a physical model which overcomes the artifacts generated in the single image dehazing by DCP method. Meng et al. [11] suggested an efficient image dehazing with boundary constraint using contextual regularization. Chen et al. [12] discussed robust image and video dehazing with visual artifact suppression via residual gradient minimization.

Various night-time dehazing methods are presented [13-17]. Anucti et al. [13] suggested fusion-based night image dehazing. Zhang et al. [14] addressed night-time low illuminated images. A local air- light component generates a maximum reflectance prior, which estimates the varying air light. Li et al. [15] presented dehazing of night-time images by reducing the glow effects and artifacts, but the image's contrast is affected. Dehazing of day and night time images is discussed in the studies [18-20]. Ancuti et al. [21] introduced a novel method to improve daytime and hazy night-time images. It estimates the ambient light on local patterns with small size tracts and not the whole image. At night, the illumination originates from several unnatural, non-uniform sources. The problem in selecting patch size is overcome by fusing more samples of inverted images using Laplacian decomposition. Xie et al. [19] have addressed dehazing algorithm, which uses dark channel prior and multi-scale retinex. On combining the dark channel prior, they recovered a quality output image but still, in processing, obtained poor form of transmission map.

Different Retinex methods are discussed in the studies [22-25]. The homomorphic filter method [22] is presented but fails to address the halo issues. The SSR algorithm [23] of the center and surround method using Gaussian kernel was introduced, resulting in increased computational complexity. To overcome these difficulties in removing turbidity using multi-scale Retinex, Guo et al. [24] proposed a method by suppressing the luminance component. Still, unfortunately, this algorithm leads to strong color distortion. Multi-scale Retinex with a colour restoration (MSRCR) scheme [25] have been suggested to eliminate the color distortion of MSR.

In image processing, non-local means techniques have been demonstrated to recuperate pictures containing surfaces successfully and are generally utilized in grayscale handling. The primary thought is to use comparative squares throughout the picture to appraise the present pixel esteem. Gilboa and Osher [26] bound together with the non-local mean approach into a regularization system by characterizing a non-local Total Variation (TV) model, in particular, the Non-local Total Variation (NL-TV) model-L1, NL-TV-L2 including models and Generalized Model of Total Non-local Variation (NL-TVG), individually, proposed calculations. From that point forward, Buades et al. [27] summed up non-nearby technique and proposed a notable neighbourhood denoising filter, particular non-local mean (NLM). The NL-TV model can safeguard both edge and textures, with great application impact. The conventional NLM strategy joined with variational retinex investigates image similarities for noise expulsion by supplanting the nearby correlation of individual pixels with the non-local examination of image patches [28]. Zosso et al. [29] proposed a unified framework by merging TV regularization with NLM retinex technique. Chung et al. [30] presented a novel white patch-based retinex-based modified dark channel prior technique for dehazing single images observed during daytime.

Ancuti et al. [31] resolved a novel submerged image enrichment utilizing different fusion methods and further developed the low light pictures caught underwater. Li et al. [32], Al-Hashim and Al-Ameen [33] and Wang et al. [34] and Park et al. [35] examined different low light improvement strategies and noise removal procedures. Guo et al. [36] proposed a Low-light Image Enhancement Method (LIME) to take advantage of the illumination design by evolving the smoothing model. Gupta and Agarwal [37] proposed another color differentiation upgrade approach for dim images with non-uniform brightening in the HSI space. The luminance part I in the HSI color space is isolated and irrelevant to the chrominance part H of an image and further enhances the image details. Rivera et al. [38] utilized an adaptive transformation function for augmentation low light images, but failed for recovery of data from shadow regions.

The DCP technique is simple but more efficient single image dehazing algorithm. Nonetheless, it ineffective in processing sky images and involves acute computations. A few better algorithms [39-43] are proposed to eradicate the shortcoming of the DCP approach. For effectiveness, He et al. [39], Zhu et al. [40], Xiao and Gan [41], Adams et al. [42] supplant the tedious DCP approach soft-matting with guided joint bilateral filtering and guided image filtering by adaptive filtering and standard median filtering, fast high-dimensional filtering respectively. Single image dehazing is discussed by Ancuti et al. [43] using D-Haze dataset. Wang et al. [44] applied the multi-scale convolutional networks that accomplish an end-to-end trainable model and can naturally distinguish hazy regions and retrieve poor texture details. Ren et al. [45] developed a multiscale deep neural network for single image dehazing by learning the mapping between haze images and their transmission maps. The proposed technique comprises a coarse-scale net that predicts a comprehensive transmission map given the whole image and a fine-scale net that locally refines desired output image. Kimmel et al. [46] proposed a variational model for the retinex problem by utilizing the spatial correlation that exists in the reflectance and illumination images. Rudin et al. [47] introduced the total variation (TV) regularizer which is very effective in recovering edges of images.

The low-light images suffer from two main problems such

as low-visibility and noises. Though the image enhancement algorithms increase the visibility, the noises in the images also increase. Most of the noise removal techniques remove the edge information which degrades the quality of the images. The retinex based algorithms are performed poorly with the unnatural images. The main disadvantage of multi-scale retinex is that they are unable to remove the halo effects near strong edges. Also, it is very important to remove the haze in both day and night time hazy images and enhancement of low-light images. To attain this and remove the drawbacks in the existing systems, DCP and non-local retinex algorithms are combined to enhance contrast and preserve edges as well.

3. PROPOSED WORK

This paper suggests a novel method for dehazing both day and night images and low light (LoL) enhancement by fusing DCP and non-local retinex (NLR). Light plays an essential role on dehazing in colour images. How select atmospheric light value is a challenging problem. In our work, the new value is obtained by first estimating the top 0.1 percentage of the brightest pixels in the dark channel, which mostly is an opaque and hazy portion of the scene. Then the retinex component of the image is computed using non-local differential equations. The following Figure 1 shows the schematic diagram of the proposed method.

The proposed method includes steps as follows:

- The dark channel prior I^{dark} is computed in opaque part of the image on the brightest track.
- Compute the non-local retinex of the low light or hazy image $\hat{r}$.
- Evolve the prior, which is obtained by combining I^{dark} and $\hat{r}$.
- Next, we computed the atmospheric light Â.
- Then initial transmission τ (x) is computed.
- Refined transmission $\tilde{\tau}$ computation guided filter.

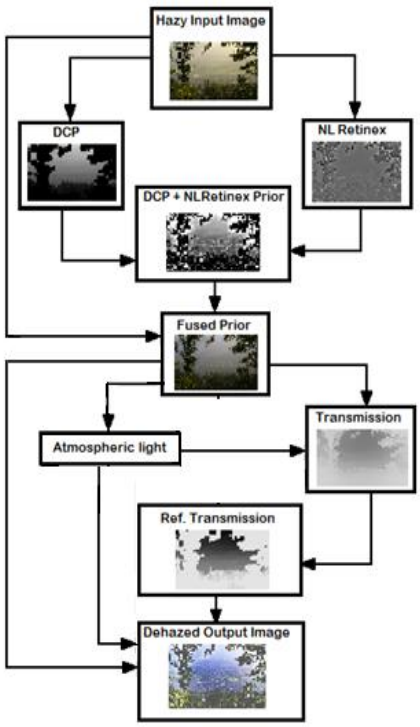

Figure 1. Schematic diagram of proposed method

- haze-free or LoL enhanced output images are obtained

$$J(x) = \frac{I(x) - \hat{A}}{max(\tilde{\tau}(x), \text{to})} + \hat{A}$$

In this work, a total average of dark channels pixels and NLR are computed and are used before estimating atmospheric light. This technique drives away the shortfall of the DCP and diminishes the artifacts of bright elements on the whole image.

3.1 Modeling haze image-atmospheric scattering model

3.1.1 Daytime haze imaging model

The optical atmospheric attenuation model [1] represents the hazy image. Figure 2 shows the atmospheric scattering model. From He et al. [1] the equation of that model is given by

$$I(x) = J(x)\tau(x) + (1 - \tau(x))A \quad (1)$$

where, I is the captured haze image, A is an ambient light, J is the true radiance, and τ is the scene transmission parameter to be evaluated.

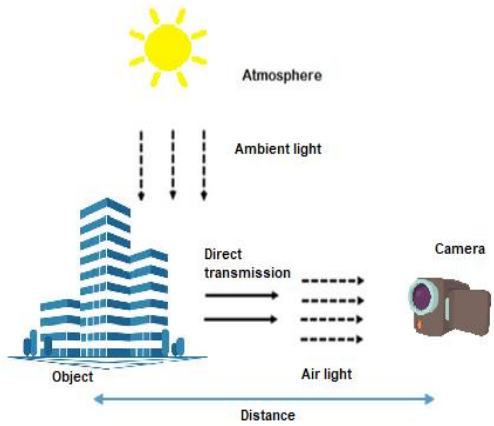

Figure 2. The daytime atmospheric scattering model

The transmission map is evaluated using equation which is given by

$$\tau(x) = e^{-\beta \cdot d(x)} \quad (2)$$

where, β is the scattering parameter and *d(x)* is the distance between the object and camera.

3.1.2 Reflectance prior

We propose a prior which depends on evaluating haze-free image patches observed during daytime. Generally, in most image patches, each color channel has huge intensities at certain pixels, and the maximum powers in such a patch have high grayscale values. Based on this an image *I,* the prior can be mathematically defined as

$$\rho_{\max^{\lambda}} = \max_{j \in \Omega} I_j^{\lambda} = \max_{j \in \Omega} L_j R_j^{\lambda} \quad (3)$$

where, ρ_{max}^{λ} is the maximum intensity in patch Ω at colour channel λ, L_j is the light intensity that falls on object surface, and R_{λ}^{j} is the reflectance. For images captured in the daytime, which are clear and visibly vivid, there is uniform light

intensity, and hence L_j is assumed to be unity. Therefore, the pixels with maximum intensity in the local patch at a particular color channel indicate the objects with high reflectance. So Eq. (3) has the following equivalent form

$$\rho_{\max^{\lambda}} = \max_{j\in\Omega} I_j^{\lambda} \tag{4}$$

The objects such as sky, road, windows of buildings, flowers, surfaces with various colors and soon have maximum reflectance. Since in most of haze-free daytime image patches, the above mentioned objects are common in the outdoor scenes, each color channel have a maximum intensity value of unity, i.e.,

$$\rho_{\max^{\lambda}} \approx 1 \tag{5}$$

In like manner, the derived perception is called as the maximum reflectance prior.

3.1.3 Nighttime haze imaging model

Eq. (1) indicates the ambient light A is supposed to be the only light source for daytime haze atmosphere. Hence similar attenuation characteristics exist for all channels, which means the captured image is independent of the wavelength. However, night-time scenes naturally consist of several colored light sources with different wavelengths, emerging in a non-uniform varicoloured ambient illumination. Hence the local ambient illumination is added to day-time haze imaging model to obtain the night-time hazy imaging model as follows:

$$I^{\lambda} = J^{\lambda}t + A^{\lambda}(1-\tau) \tag{6}$$

where, I^{λ} is the observed image, J^{λ} is the scene radiance for the corresponding wavelength. But the scene radiance depends on ambient light A^{λ} and reflection R^{λ} i.e., $J^{\lambda} = A^{\lambda}R^{\lambda}$.

$$I^{\lambda} = A^{\lambda}R^{\lambda}t + A^{\lambda}(1-\tau) = L\eta^{\lambda}R^{\lambda}t + L\eta^{\lambda}(1-\tau) \tag{7}$$

where, L represents the illumination intensity and η^{λ} is the colour of ambient illumination.

3.1.4 Estimation of reflectance prior for night image

In the hazy night-time scenario, lights emitted from several light sources vary steadily in space, except for some obstructions, which causes abrupt changes among dark and luminous regions. In the whole image, such extremities are sparse. Hence, Fogg scatters light in multiple directions and synthesizes smoothly varying ones. So, we assume the ambient illumination A^{λ}_j on each local patch j ∈ Ω to be constant. We also assumed τ to be a constant on Ω and written as τ_{Ω}. Following the assumptions, on maximizing both side of Eq. (3), we get

$$\begin{aligned} \rho^{\lambda}_{max} &= \max_{j\epsilon\Omega} I_j^{\lambda} \\ &= \max_{j\epsilon\Omega}(L^{\lambda}_{\Omega}\eta^{\lambda}_{\Omega}R^{\lambda}_j t_{\Omega} + L^{\lambda}_{\Omega}\eta^{\lambda}_{\Omega}(1-\tau_{\Omega})) \\ &= \max_{j\epsilon\Omega} R^{\lambda}_j(L^{\lambda}_{\Omega}\eta^{\lambda}_{\Omega}t_{\Omega} + L^{\lambda}_{\Omega}\eta^{\lambda}_{\Omega}(1-\tau_{\Omega})) \end{aligned} \tag{8}$$

From Eq. (4), we have $\max_{j\in\Omega} R^{\lambda}_j \approx 1$. Substitute into the above equation. We have the proposed maximum reflectance prior

$$\rho^{\lambda}_{max} = L^{\lambda}_{\Omega}\eta^{\lambda}_{\Omega}t_{\Omega} + L^{\lambda}_{\Omega}\eta^{\lambda}_{\Omega}(1-\tau_{\Omega})) = L^{\lambda}_{\Omega}\eta^{\lambda}_{\Omega} \tag{9}$$

Thus, the reflectance of the night- time image is the function of ambient light intensity and color. So it is different from the day image. During the night, the A^{λ} is multi-colored and varying. So, for hazy night image patches, the maximum intensities at each colour channel will have maximum reflectance due to the light sources. By using this proposed prior, our method reduces artifacts. We generalized this idea and proposed a novel prior to performing day and night-time image dehazing and low light enhancement. We first use non-local retinex to compute the reflectance prior, enabling us to estimate ambient illumination's color map. Then, computing the transmission estimate and the guided filter determines its refined version. Finally, a haze-free image with good contrast is obtained. The following section estimates the proposed reflectance prior to using the non-local retinex method.

3.2 Dark channel prior estimation

From Eq. (1), it is understood that to restore the image without haze, it is essential to acquire the $\tau(x)$ and the A. To evaluate the $\tau(x)$, He [2] proposed an optimum method based on the dark channel prior. It is mentioned that in haze-free non-sky outdoor images, among any red-green-blue color channels, at least there is one channel that might have the lowest intensity at some pixels. i.e.,

$$J^{dark}(x) = \min_{c\,\epsilon[r,g,b]}\left(\min_{y\epsilon\Omega(x)}(J^{C}(y))\right) \approx 0 \tag{10}$$

where, J^{dark} specifies the dark channel of J(x), J^{C} is the colour channel of J(x), and $\Omega(x)$ is a petite tiny portion that is surrounding the pixel x. Ultimately we intend to enhance the low- intensity hazy image I and generate a visibly good and improved radiance J.

a b c d e

Figure 3. Dark channel prior if Hazy day input images a) Hill tree b) Building c) Retinex d) Swan d) Stadium and e) Bench

a b c d e

Figure 4. Dark channel prior if Hazy night input images a) Bus b) Tower c) Van d) Scooter and e) Park booth

The experimental results of dark channel for different input hazy images are shown in Figure 3 and Figure 4 for day images and night images, respectively. The existence of high levels of shadow, colorful objects, and dark objects in the hazy image causes variation of dark channel values.

3.3 Non-local retinex

Atmospheric light is not uniform and constant for hazy night images, as night scenes often contain multiple light sources. Often lit and non-illuminated regions have different color characteristics and cause total variation color distortion and halo artifacts. We propose a non-local retinal model based on the L^2 norm to overcome this problem.

3.3.1 Non-local mean filtering

This section estimates the retinex-based reflectance prior to using a unified method that combines non-local means with TV regularization technique. To smooth an image, normally, local mean filters consider the average value of a number of pixels around target pixel. But non-local mean (NLM) filters compute the mean value of the target pixel considering all the weighted pixels in the whole image. The weight is computed by how much color similarity exists between these pixels and the target pixel. This leads to high clarity and less loss of information. Also, the most similar pixels for the target pixel need not to be located closer. Hence, it is important to scan a vast image area for those pixels that resembles the target pixel. The self-similarity is measured by equating an entire patch surrounding each pixel. The NLM filtering performs a non-local comparison of image patches that inspects image self similarities for removing noise. Hence, for a given noisy image *I,* the restored intensity ***u*** of the pixel at (*x*, *y*) is presented as

$$u(x,y) = I_{NL}(x,y) = \frac{\sum_{(m,n)\in\Omega} I(m,n).w(x,y,m,n)}{\sum_{(m,n)\in\Omega} w(x,y,m,n)} \qquad (11)$$

where, NL denotes the nonlocal means, and Ω-is a search window. The weight *w(x, y, m, n)* specifies the similarity between two pixels at (*x*, *y*) and *(m, n)* is evaluated by

$$w(x,y,m,n) = exp\left(-\frac{\| I(P(x,y)) - I(Q(m,n)) \|_{2,a}^2}{h^2}\right) \qquad (12)$$

where, *h* represents a filter order parameter, *P*(*x*, *y*) and *Q(m, n)* are the two image patches centered at (*x, y*) and *(m, n)* respectively; $||I\ (P(x; y))$ - $I\ (Q(m, n))||_2^2$ means the weighted Euclidean distance between two image patches *P*(*x, y*) and *Q(m, n*)of the input image *I(x,y)*.

3.3.2 Variational retinex

Kimmel et al. [46] present a variational retinex formulation as $u = r + i$ where $i = \log(I)$, $r = \log(R)$, and $u = \log(u)$ using the same assumption in PDE formulations. The retinex is

$$r = \arg\min_u \int_\Omega |\nabla u|^2 + \alpha |u-i|^2 + \beta |\nabla(u-i)|^2 \qquad (13)$$

But the above conventional regularizer is not an efficient method for image restoration problems.

Rudin et al. [47] introduced the total variation (TV) regularizer, which is very effective in recovering edges of images. This resembles with the PDE-based algorithms. Buades et al. [27] proposed a nonlocal mean method. Then Gilboa and Osher [26] introduced the nonlocal TV regularizer, the most popular optimization method for processing textured images. We can define the nonlocal weight between two pixel x and y in different patches with a patch size of Ω for a given image u(x),

$$w_h(x,y) = exp\left\{\frac{-G_a * (u(x)-u(y))^2}{2h^2}\right\} \qquad (14)$$

where, G_a is the Gaussian kernel. After computing nonlocal weights, the nonlocal gradient operator $\nabla_w u(x,y)$ is obtained as partial difference vector at *x*

$$\nabla_w u(x,y) = u(y) - u(x)\sqrt{w(x,y)}, \qquad \forall y \in \Omega \qquad (15)$$

and the NLTV regularizer can be defined as

$$\int_\Omega |\nabla_w u| = \iint_\Omega \left((u(y)-u(x))^2\, w(x,y)\, dy\right)^{\frac{1}{2}} dx \qquad (16)$$

So the NLTV regularized model for retinex is

$$r = arg\min_u \left\{ t\int_\Omega |\nabla_w u| + \frac{1}{2}\| \nabla(u-i) \|_2^2 \right\} \qquad (17)$$

The nonlocal gradient operator term is the TV regularizer parameter that operates to get the sharp edge information. The second term represents the L^2 norm gradient value of the reflection.

3.3.3 L^2 gradient fidelity

Our work implements a non-local retinal model based on the L^2 norm that simulates the average activity of inhibitory and excitatory neuronal populations in the cortex. This potential biological feasibility of the L^2 standard of our work is divided into two parts using a filtered gradient approach, the reflection sparse prior and the reflection gradient fidelity prior to the observed image gradient. The energy of the L^2 gradient-fidelity non-local Retinex is

$$J(r) = \left\| \nabla_w r - \nabla_{w,f} i \right\|_2^2 + \alpha \|r\|_2^2 + \beta \, \|r - i\|_2^2 \qquad (18)$$

The analogous Euler-Lagrange equations are

$$0 = 2(-\nabla_w \hat{r} + \nabla_{w,f} i \; + \alpha \, \hat{r} + \beta \, (\hat{r} - i)) \qquad (19)$$

Finally the reflectance $\hat{r}$ is estimated as

$$\hat{r} = ((\alpha + \beta) I - L)^{-1} \, (\beta \, i - \nabla_{w,f} i)) \qquad (20)$$

where, I represent the identity matrix and L is the Laplacian matrix. The parameter α and β are dynamic range compression factor that controls the degree of local contrast enhancement. This unified framework of NLTV-Retinex and DCP efficiently performs low-light enhancement and dehazing of day and night images. Figures 5 and 6 show the non-local retinex, computed using the reflectance component of given day and night images. Since, the illumination component of the image changes smoothly, the edges present in the reflectance primarily contribute to the spatial derivatives of the observed intensity.

Figure 5. Non local retinex output of hazy day input images a) hill tree b) building c) swan d) stadium and e) bench

Figure 6. Non local retinex output of hazy night input images a) bus b) tower c) van d) scooter and e) park booth

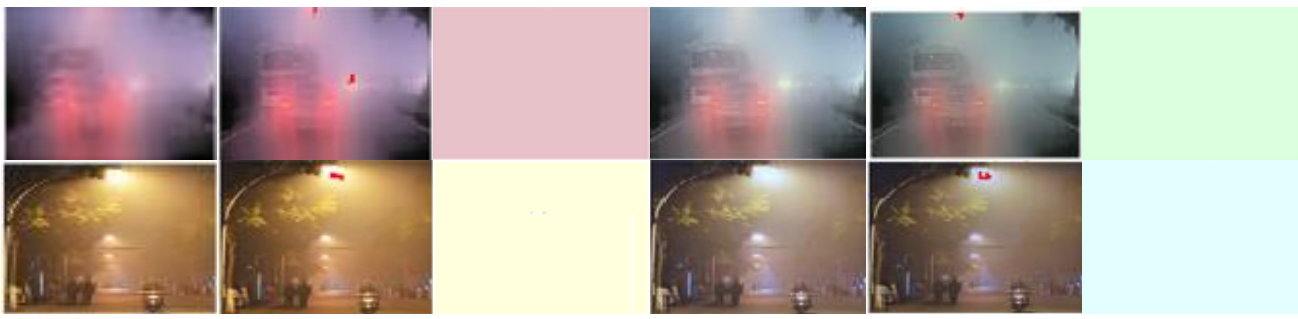

Figure 7. Evaluation of atmospheric light of night images a) hazy input image b) locating ambient light c) conventionally measured A d) fused prior (hazy image, DCP and retinex) e) locating proposed ambient light f) estimated new atmospheric light

3.4 Proposed estimation of atmospheric light

The scene's radiance is generally described by the atmospheric light (A). Generally, in the various haze removal methods on a single image, the atmospheric light A obtained is from the severely blurred region. We proposed a modified method for air-light estimation. The picture elements with the brightest intensity are usually found on white objects that appear in the real image, which may be refined for compute atmospheric light [16]. The proposed algorithm includes steps as follows:

- First DCP I^{dark} is estimated by initially identifying the top 0.1 percentage of the bright candidate pixels on brightest channel in opaque part of the image.
- Compute the non-local retinex prior of the low light or hazy image $\hat{r}$.
- Evolve the dark channel-retinex (DCR) prior, obtained by fusion of I^{dark} and $\hat{r}$.
- Whole Then combine the input image I with DCR prior and generate a new input image I′.
- Next, compute the atmospheric light Â for I′ the modified input image.

For day images assuming the contribution of atmospheric light is uniform in the whole scenario, which the observer captures, and it is evident if sunlight is present in the scene. In most of the situation, this is not necessary to be true. When fog exists, light undergoes scattering during to the night-time due to aerosols present. Thus in the foggy night, ambient light *A* does not prevail the same due to various light sources. Hence instead of *A,* we changed to A^{λ} and from which Â is computed. This is achieved by NLTV retinex, which is derived from the Laplacian operation on new input image *I′*. Then in *I′,* the pixels with the mean intensity are selected for Â, to avoid overestimation of the atmospheric light.

The atmospheric light estimation is shown in the above Figure 7 for daytime and hazy nighttime images. First, the location of atmospheric light is selected and then A estimated for the original hazy input image. Then it is compared with the new image obtained by fusing DCP and non-local retinex with input image. When analyzing the fige.7 for hazy, low light, or night time images, in which we find that if there exist brighter lights sources. So if we choose the brightest pixel for Â, it may lead to noise artifacts. Moreover, the light sources may not appear natural, and might be surrounded by halos or artifacts. To prevent such problems, we chosen bright channel based on the mean intensity estimation.

3.5 Transmission optimization

The improved atmospheric light estimation Â is utilized to evaluate the transmission map. While evaluating the estimate of the transmission map, transmission is considered persistent in the local patch Ω(x). From [2] on manipulating both sides of Eq. (1) with transmittance minimum transformation function in the RGB channels, we have

$$\min_{c\,\epsilon[r,g,b]}\left(\min_{y\,\epsilon\Omega(x)}(I^{c}(y))\right) = \tau(x).\min_{c\,\epsilon[r,g,b]}\left(\min_{y\,\epsilon\Omega(x)}(I'^{c}(x))\right) + (1-\tau(x))\hat{A}^{c} \tag{21}$$

The value of $I'^{C}(x)$ reduces to zero inside the haze-free local patch and $\hat{A}^{C}$ is invariably positive. The transmittance of sky portion or that region with uniform intensity tends to zero. In order to handle both sky and other regions in the image a constant ω is introduced into equation:

$$\tau(x) = 1 - \omega.\min_{c\,\epsilon[r,g,b]}\left(\min_{y\,\epsilon\Omega(x)}\left(\frac{I'^{c}(y)}{\hat{A}^{c}}\right)\right) \tag{22}$$

where, $0 \le \omega \le 1$. we used the patch size Ω(x) of 15 x15 for night images and 30 x 30 for day images.

The transmission map refinement is an important step in our work. The Figure 8 depicts the consolidated output parameters. In our proposed method we use fast guided fitter for the refinement of the transmission map. The guided filter (GF) is an advanced filtering technique which preserves edges and execution speed. It is because of its nice visual quality, fast speed, and ease of implementation. The definition of general linear translation variant filter [39] is shown as

$$q_i = \sum_j w_j(g).I_j \tag{23}$$

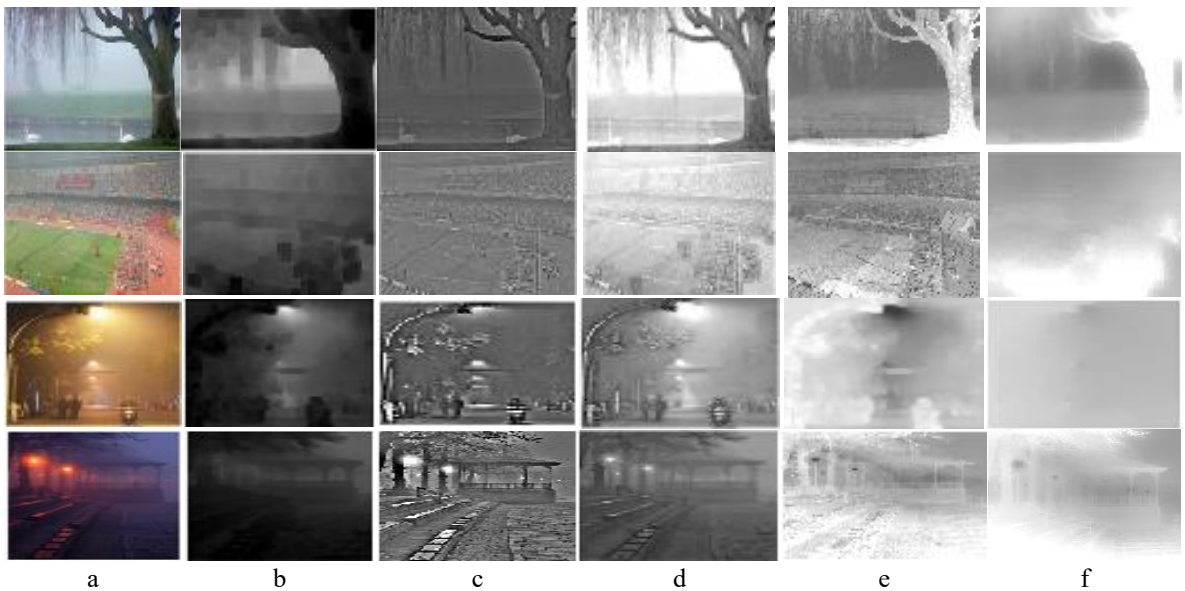

Figure 8. Consolidated outputs for both the day and night hazy input images a) Input image b) Dark channel prior c) Retinex d) Combined DCP and retinex prior e) Transmission and f) Refined transmission

where, *I(x, y)* is input image, *g(x, y)* is guide image and output image is *q(x,y)*. w_{ij} is a filter mask kernel with (i, j) representing the index of the pixels. The salient feature of GF is that it gives a linear relation between *q(x,y)* and *g(x,y)*. In our work, in order to reduce reconstruction error between *I(x,y)* and *g(x,y)* fast guided filter is shown as follows [12]:

$$q_i = a_k\, g_i + b_k, \qquad \forall\ i \in w_k \tag{24}$$

$$a_k = \frac{\frac{1}{|w|}}{\sigma_k^2 + \epsilon} \sum_{i \in w_k} g_i\, I_i - \mu_k\, \bar{I_k} \tag{25}$$

$$b_k = \bar{I_k} - a_k \mu_k \tag{26}$$

where, μ_k and σ_k^2 are the mean and variance of *g(x,y)* in window w_k. ε represents regularization parameter and $|w_k|$ is the number pixel in w_k $\bar{I_k}$ is mean of input image I(x,y) in window w_k. The consolidated outputs for both the day and night hazy input images of various blocks are presented in the above Figure 8. The guided filter successfully refines the coarse transmission output, smoothens the slope inversion artifacts, and creates outwardly satisfying edge profiles.

3.6 Scene radiance recovery

We initially select the foremost 0.1 percentage of most illuminant pixels in the dark channel and compute the retinex. Then by combining both DCP and retinex, we will get the dark channel-retinex (DCR) prior and then compute to the atmospheric light Â.

a b c d e f

Figure 9. Haze free radiance generated by various methods for both day and night hazy input images a) Input image b) He et al. c) Li et al. d) Ancuti et al. e) Chen et al. and f) Our result

After evaluating the atmospheric light (Â) and final transmission *τ(x)* from *I′(x)* scene radiance *J(x)* can be recovered. Figure 9 shows the haze free radiance generated by various methods for both day and night hazy input images. That means from the optical scattering image model of Eq. (1). We can recover the *J(x)* using the *τ(x)*. Since the parameter *J*(*x*) • *τ(x)* scene irradiance value is approximately close to zero, for the ground truth, the *τ(x)* is restricted to a minimum value of t_0, and is assigned an appropriate value of 0.1. Hence haze-free output image *J(x)* is evaluated by

$$J(x) = \frac{I'(x) - \hat{A}}{\max\left(\tau(x), to\right)} + \hat{A} \tag{27}$$

It is observed from the above output images that our algorithm using combined DCP and non-local derivative retinex results in the effective pixel-wise blending with both advantages of DCP and retinex.

4. RESULT ANALYSIS

4.1 Qualitative analysis - day image

To evaluate the efficacy, and quality of our proposed method, we analogize our approach with some up-to-date algorithms in both subjective and objective aspects. Those algorithms we select for comparison include He et al. [1], Fattal [8], Cai et al. [9], Chen et al. [12], Ancuti et al. [13] and Li et al. [15]. Experiments have been performed in Matlab R2020b on a personal computer with a 2.60 GHz Intel pentium dual-core processor and 4G RAM.

Figure 10 shows the comparison of our proposed method with existing methods. It can be seen that DCP [2] tends to over-dehaze the light source regions while under-dehaze the dark areas. On the contrary, retinex preserves shapes and edges in illuminated area, while the dark areas seem over-enhanced. The proposed result obtained by combined DCP and non-local retinex give is very effective. We applied our proposed technique to many classical standard testing photos in our experiments. The robustness of proposed model is demonstrated by comparing our results with the existing algorithms.

Our technique is a single image approach. It first generates DCP and NLTV retinex and fused together to generate new prior using a single image, not multiple images. This newly generated prior combined with the input image. We use different patch size for day and night images to determine the airlight values. Our proposed method improves the overall visibility and contrast of the image, thereby transforming the image into a more suitable form for human observation and computer analysis.

4.2 Qualitative analysis - night image

This section compares and discusses our results for dehazing nighttime hazy images with existing state-of-the-art nighttime methods. Only a few types of research are available in the literature. We choose small patch sizes 15 x 15 for night image, thereby avoiding computation of the ambient light from veil of several light sources. Otherwise, the image obtained might result in poor contrast.

From the Figure 11, our algorithm performs better than other algorithms by better visibility and contrast. On comparing with the study [13], our algorithm restores the color balance without overwhelming brightness and fewer artifacts. Though, the output of the study of Li et al. [15] reduces the glow effect and halos contrast is poor than our result. Our proposed algorithm have better colour balance and preserve colour better than other algorithms [2, 12].

4.3 Quantitative result analysis -day image

A specific number of hazy daylight images of O-Haze dataset are analysed in Figure 12 in terms of PSNR, SSIM, and CIEDE2000 [43]. The performance metrics PSNR, SSIM, and CIEDE2000, are measured for the low-light image O-Haze dataset and are tabulated below. The parameters are measured by comparing the output with the ground truth.

a b c d e f

Figure 10. Comparison of output results of on analysing hazy day input images. a) Input image b) He et al. [1] c) Li et al. [15] d) Ancuti et al. [13] e) Chen et al. [12] and f) Our result

a b c d e f

Figure 11. Comparison of output results of on analysing hazy night input images. a) Input image b) He et al. [1] c) Li et al. [15] d) Ancuti et al. [13] e) Chen et al. [12] and f) Our result

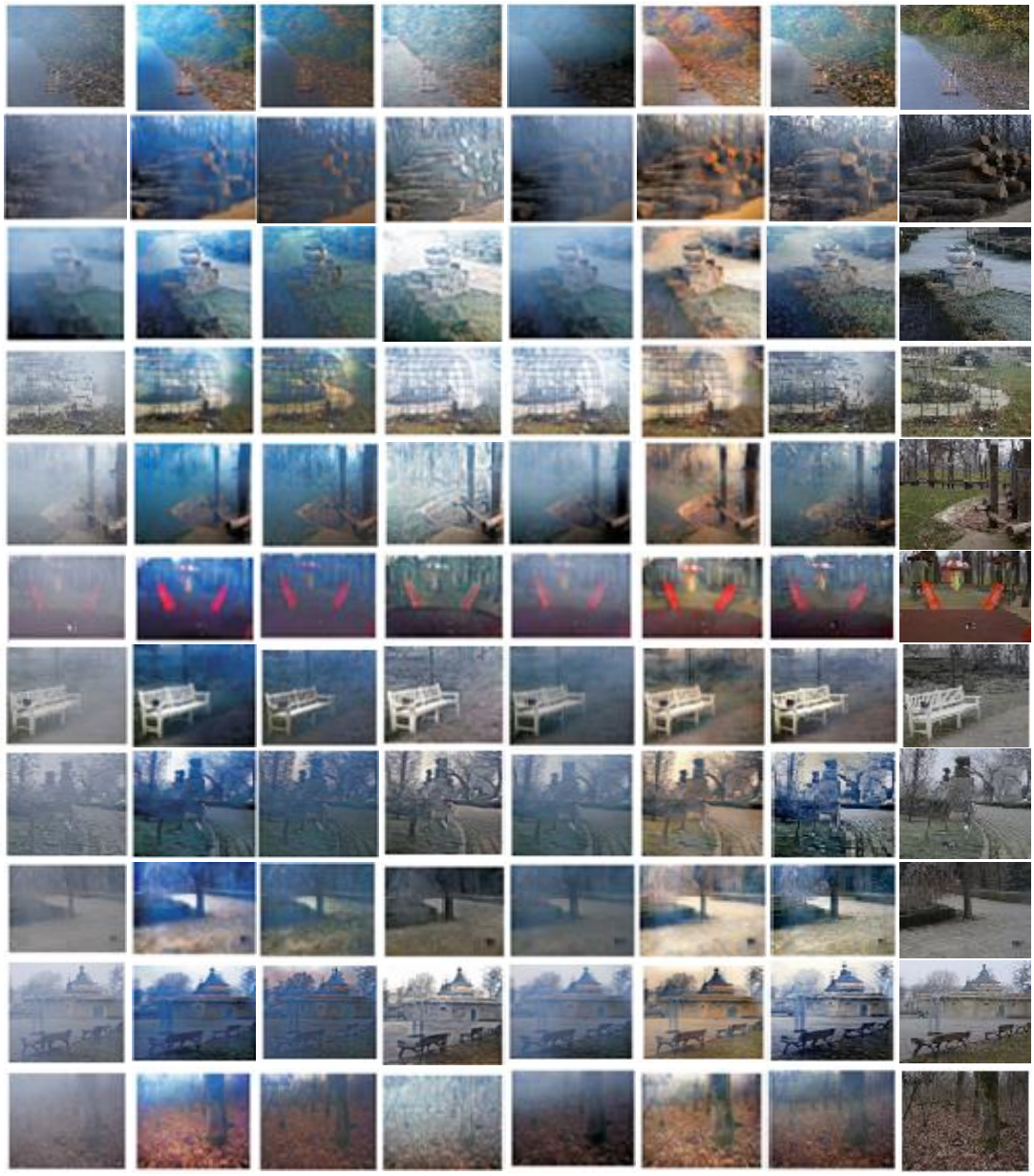

Figure 12. Comparison of results on analyzing the O-Haze dataset images a) Hazy input image b) He et al. [1] c) Cai et al. [9] d) Fattal [8] e) Meng et al. [11] f) Ancuti et al. [13] g) our result and h) ground truth

The proposed method is compared with existing algorithms and evaluated by analyzing of O-Haze data set images. It consists of 45 pairs of hazy images and its ground truth with an image of size 800 X 600. The quantitative parameters PSNR, SSIM, and CIEDE2000 for daytime Hazy outdoor dataset O-HAZE are measured. The results and parameters PSNR, SSIM, and CIEDE2000, are compared with the ground truth values. From Table 1 of the above analysis, we found that the input image_01 PSNR of our algorithm is 23% better than Cai et al. [9], 22% better than Fattal [8], and 7% better than He et al. [1]. SSIM of our algorithm is 24% better than Cai et al. [9], 9% better than Fattal [8], and 7% better than Ancuti et al. [13]. Similarly, the CIEDE2000 parameter of our algorithm is 18% better than He et al. [1], 25% better than Cai et al. [9] and Fattal [8], 9% better than Ancuti et al. [13]. On comparing the image_19 PSNR of our algorithm is 16% better than He et al. [1], 12% better than Cai et al. [9], 29% better than Fattal [8], 21% better than Ancuti et al. [13]. SSIM of our algorithm is 9% better than Cai et al. [9], 2% better than Ancuti et al. [13]. Similarly, the CIEDE2000 parameter of our algorithm is 27% better than Fattal [8], 9% better than Cai et al. [9], and 4% better than He et al. [1]. The color difference between the output and GT is less when the CIEDE2000 value is less, which means the quality of the image is good. Similarly the higher the value of the PSNR and SSIM better the quality. The average value of the parameters of our results is better than others work. So it is obvious that our work outperforms He et al. [1], Fattal [8], and Cai et al. [9] algorithm on evaluating the D-HAZE dataset.

4.4 Quantitative result analysis –low light/dark image

The LOL dataset is a benchmark designed to enhance images captured in dark, poor light environment. The LOL dataset consists of 500 low-light and normal-light image pairs. The LOL dataset is divided into 485 training pairs and 15 testing pairs. The images are 400x600 pixels in resolution. We intend to exploit the quality of non-local retinex to process low light dark image without going for gamma correction and to prove the effectiveness of our proposed technique which

performs three different tasks vis-a-vis both day/night image dehazing and low light enhancement. It is rare to find single method to perform three different functions in literature. Our proposed method improves the overall visibility and contrast of the image. For result analysis, we used the available author's source code. Figure 13 demonstrates the low light enhancement techniques of Chen et al. [12], Li et al. [15], He et al. [1], and Ancuti et al. [13] and our results compared with ground truth of the low light dataset (LOL).

Figure 13 directly compares our approach with the recent specialized techniques of Li et al. [15], Chen et al. [12], and Ancuti et al. [13]. Li et al. [15] tends to darken the original image and to over-amplify colours in some regions. We used inversed version of the original DCP source code of He et al. [1], and we got the LoL analysis output with modified code; otherwise, it could have been dark output for all most all images. So Li et al. [15] and Chen et al. [12] algorithms performing good in daytime image enhancement also have poor visibility and less image enhancement. In general, existing techniques cannot enhance the image's dark veil and are poor in restoration. Only Ancuti et al.'s [13] work and our results performed good on LoL image enhancement. The results are compared with ground truth pair of dark LoL image.

From Table 2 of the analysis, we found for the set-35 image, PSNR of our algorithm is 32% better than He et al. [1], 64% better than Chen et al. [12], and 72% better than Li et al. [15]. SSIM of our algorithm is 23% better than He [2], 60% better than Chen et al. [12], 80% better than Li et al. [15]. Similarly CIEDE2000 parameter of our algorithm is 28% better than He [2], 61% better than Chen et al. [12], 66% better than Li et al. [15]. So it is obvious that our work outperform the existing systems by He et al. [1], Chen et al. [12] and Li et al. [15] algorithms using LOL image dataset. On comparing the LoL_imageset_258 our work is the PSNR is 15%, SSIM 20% and CIEDE2000 14% better than Ancuti t al. [13] algorithm and better than Ancuti's algorithm. The color difference between the output and GT is less when the CIEDE2000 value is less, which means the quality of the image is good. Similarly the higher the value of the PSNR and SSIM better the quality. The average value of the parameters of our results is better than others work.

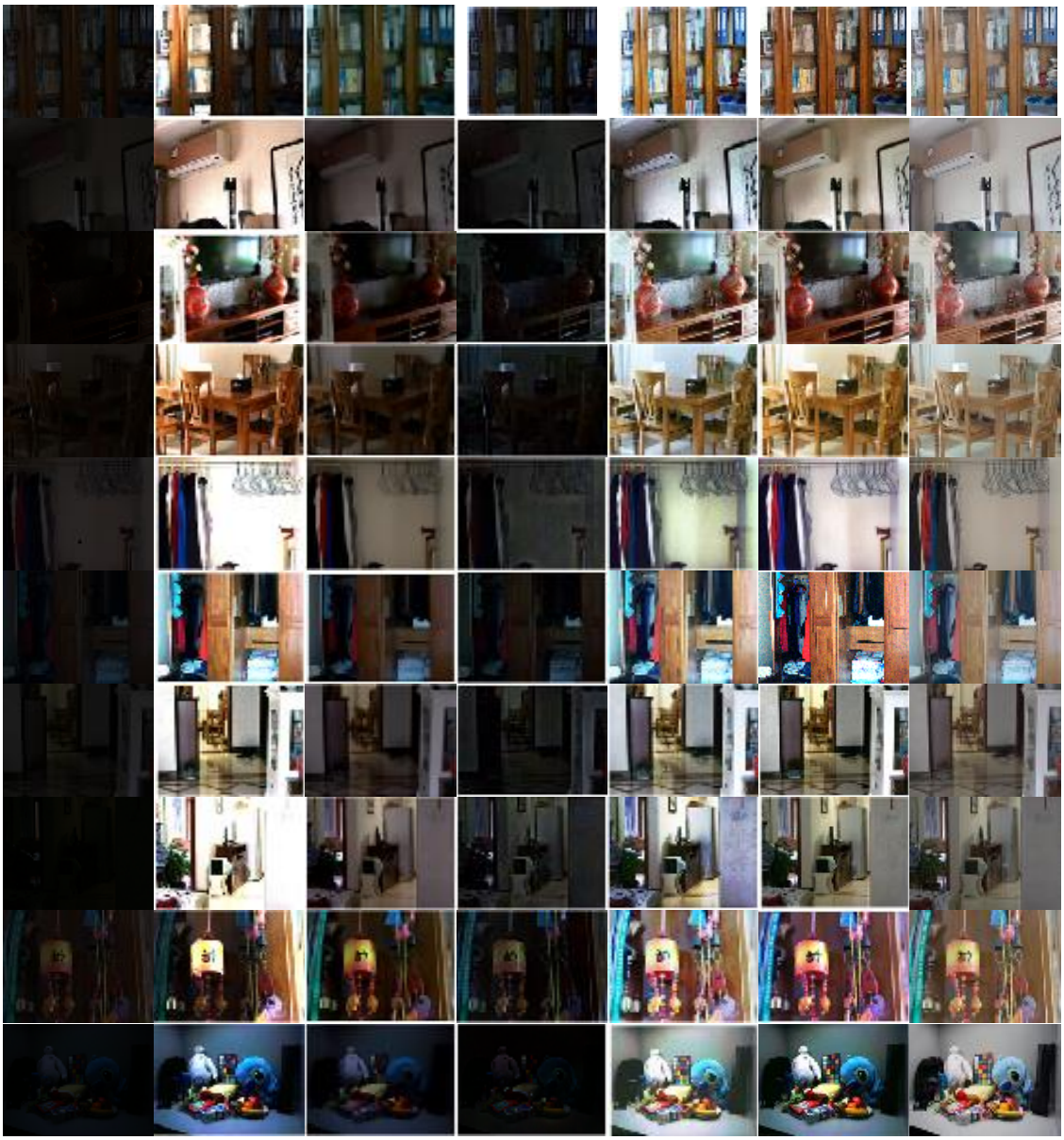

Figure 13. Comparison of results on analyzing the LOL (low light) dataset images a) input image b) He et al. [1] c) Chen et al. [12] d) Li [15] e) Ancuti et al. [13] f) our result and g) ground truth

Table 1. The quantitative parameters PSNR, SSIM, and CIEDE2000 measurements for day time Hazy low light image dataset LOL. Reference parameter courtesy- of Cosmin Ancuti et al.

OHaze Dataset	**He et al. [1] result**			**Cai et al. [9] result**			**Fattal [8] result**			**Ancuti et al. [13] result**			**Our result**		
Input Image	PSNR	SSIM	CIEDE 2000	PSNR	SSIM	CIEDE 2000	PSNR	SSIM	CIEDE 2000	PSNR	SSIM	CIEDE 2000	PSNR	SSIM	CIEDE 2000
01	15.64	**0.82**	22.37	13.01	0.58	24.42	13.24	0.73	24.29	**17.27**	0.75	20.09	16.76	**0.82**	**18.48**
06	16.68	**0.74**	19.00	15.32	0.59	16.16	15.16	0.73	21.89	15.76	0.68	**15.53**	**17.47**	0.67	15.55
10	16.22	0.78	15.22	15.02	0.71	16.17	16.42	0.75	17.49	14.49	0.73	19.21	**16.86**	**0.80**	**15.14**
19	15.69	**0.81**	16.31	16.27	0.72	16.92	13.87	0.79	21.45	14.63	0.78	15.12	**18.47**	**0.81**	**14.73**
20	16.49	0.61	23.81	13.69	0.50	23.71	15.62	0.62	20.73	**18.01**	**0.78**	**12.67**	16.47	0.66	18.74
21	16.78	0.69	27.50	16.37	0.71	19.49	16.10	0.63	28.25	**19.49**	**0.78**	**10.72**	18.87	0.75	16.38
27	13.60	0.61	21.38	15.21	0.64	17.16	14.18	0.67	22.37	**19.02**	**0.77**	**10.94**	17.36	0.76	13.92
30	15.71	0.75	18.85	18.57	0.77	12.70	14.68	0.72	18.46	**21.51**	**0.83**	**11.25**	20.35	0.82	13.30
33	18.16	0.76	18.54	17.87	0.81	14.61	17.28	0.76	17.86	12.15	0.61	20.86	**18.31**	**0.85**	**14.13**
41	15.42	0.77	19.54	20.03	**0.84**	12.78	12.52	0.66	23.71	18.97	0.84	13.02	**21.19**	**0.84**	**12.77**
42	15.47	0.79	19.70	16.35	0.58	15.58	17.63	0.73	**13.21**	14.60	0.74	15.37	**17.80**	**0.82**	**12.52**

Table 2. The quantitative parameters PSNR, SSIM, and CIEDE2000 measurements for day time Hazy low light image dataset LOL

LOL Image Dataset	**He et al. [1] result**			**Chen et al. [12] result**			**Li et al. [15] result**			**Ancuti et al. [13] result**			**Proposed system**		
IP Image	PSNR	SSIM	CIEDE 2000	PSNR	SSIM	CIEDE 2000	PSNR	SSIM	CIEDE 2000	PSNR	SSIM	CIEDE 2000	PSNR	SSIM	CIEDE 2000
05	10.68	.4719	33.51	11.49	.5587	29.70	08.31	.3231	43.53	**19.85**	**.7501**	**14.71**	19.14	.7457	15.29
14	16.47	.4926	21.93	07.42	.4411	43.90	05.70	.2212	49.31	15.26	.5236	21.58	**18.48**	**.5368**	**15.68**
35	15.49	.5479	22.39	08.30	.2823	41.08	06.59	.1417	47.95	**22.13**	**.6917**	**15.54**	21.57	.6837	16.24
56	15.94	.4312	22.76	07.98	.2778	40.57	06.44	.1129	46.84	**22.73**	**.5890**	**14.72**	21.76	.5784	16.42
64	15.28	.4934	28.24	07.87	.3469	44.57	06.11	.1421	48.67	19.75	.6032	18.95	**20.18**	**.6241**	**19.55**
145	09.64	.6904	32.03	13.68	.6509	21.86	08.85	.3418	38.14	16.65	.5241	20.03	16.59	.6423	20.06
191	17.35	.5472	22.97	09.87	.3849	36.27	07.41	.1987	40.62	19.31	.6349	18.51	**20.05**	**.6662**	**18.13**
239	12.56	.5346	25.22	13.67	.5972	22.71	09.77	.2750	34.78	15.35	.6266	19.90	**19.78**	**.6568**	**13.66**
243	08.27	.5430	45.44	21.75	.8035	10.12	12.50	.4927	26.29	13.58	.5549	23.42	**18.69**	**.7668**	**12.80**
258	12.24	.5024	29.82	12.29	.5378	27.94	09.14	.2777	41.53	17.30	.6346	22.89	**20.67**	**.7811**	**19.06**
487	12.86	.5026	29.11	07.64	.2172	43.43	06.13	.1725	49.54	**20.99**	**.5582**	**16.39**	20.38	.5427	17.19
538	13.57	.4059	26.26	07.51	.2526	45.91	06.31	.1388	50.52	**21.58**	**.5864**	**16.69**	21.47	.5792	17.11
590	08.15	.4918	36.36	12.14	.8038	22.21	10.68	.6258	25.29	**14.88**	**.7875**	**19.75**	14.54	.8147	20.17
738	11.85	.5088	26.82	14.02	.4464	23.38	11.51	.4012	30.11	15.61	.6141	20.91	**19.23**	**.7017**	**15.02**
782	12.16	.3965	27.88	11.28	.3492	31.25	09.57	.2682	36.39	15.83	.6674	22.43	**16.87**	**.7245**	**17.97**

5. CONCLUSIONS

The method proposed here can dehaze an image independent of whether it was captured during the day or night. We intend to exploit the quality of non-local retinex to process low light dark image without going for gamma correction and to prove the effectiveness of our proposed technique which performs three different tasks vis-a-vis both day/night image dehazing as well as low light enhancement. It is rare to find a single method to perform three different tasks in literature. We estimated the non-local patches that contributed to airlight and performed dehazing. Using the same non-local retinex, we remove the effect of airlight to obtain enhanced LoL image from the dark LoL input image. From the above analysis we found for the image set-35 image, PSNR of our algorithm is 32% better than He et al. [1], 64% better than Chen et al. [12], and 72% better than Li et al. [15]. SSIM of our algorithm is 23% better than He et al. [1], 60% better than Chen et al. [12], and 80%better than Li et al. [15]. Similarly CIEDE2000 parameter of our algorithm is 28% better than He et al. [1], 61% better than Chen et al. [12], 66% better than Li et al. [15]. So it is obvious that our work is outperforms He et al. [1], Chen et al. [12], and Li et al. [15] algorithm in evaluating the LOL image dataset. On comparing the images-258, our work shows the PSNR is 15%, SSIM 20%, and CIEDE2000 14% better than Ancutis et al. [13] algorithm. Hence our method performs better than existing methods. Generally, when the CIEDE2000 value is less, the color difference between the output and GT is less, which infers that the quality of the image is good. Similarly, the higher the value of the PSNR and SSIM better the quality. The average value of the parameters of our results is better than others work. In the future, we will be using a convolutional neural network to enhance the performance.

REFERENCES

[1] He, K., Sun, J., Tang, X. (2010). Single image haze removal using dark channel prior. IEEE Transactions on Pattern Analysis and Machine Intelligence, 33(12): 2341-2353. https://doi.org/10.1109/TPAMI.2010.168

[2] Chung, Y.L., Chung, H.Y., Chen, Y.S. (2020). A study of single image haze removal using a novel white-patch retinex-based improved dark channel prior algorithm. Intelligent Automation and Soft Computing, 26(2): 367-383. https://doi.org/10.31209/2020.100000206

[3] He, K., Sun, J., Tang, X. (2010). Single image haze removal using dark channel prior. IEEE Transactions on Pattern Analysis and Machine Intelligence, 33(12): 2341-2353. https://doi.org/10.1109/TPAMI.2010.168

[4] Narasimhan, S.G., Nayar, S.K. (2002). Vision and the atmosphere. International Journal of Computer Vision, 48(3): 233-254. https://doi.org/10.1023/A:1016328200723

[5] Li, B., Wang, S., Zheng, J., Zheng, L. (2014). Single image haze removal using content-adaptive dark channel and post enhancement. IET Computer Vision, 8(2): 131-140. https://doi.org/10.1049/iet-cvi.2013.0011

[6] Pal, T. (2018). Visibility enhancement of fog degraded image sequences on SAMEER TU dataset using dark channel strategy. 2018 9th International Conference on Computing, Communication and Networking Technologies (ICCCNT), pp. 1-6. https://doi.org/10.1049/iet-cvi.2013.0011

[7] Berman, D., Treibitz, T., Avidan, S. (2018). Single image dehazing using haze-lines. IEEE Transactions on Pattern Analysis and Machine Intelligence, 42(3): 720-734. https://doi.org/10.1109/TPAMI.2018.2882478

[8] Fattal, R. (2014). Dehazing using color-lines. ACM Transactions on Graphics (TOG), 34(1): 1-14. https://doi.org/10.1145/2651362

[9] Cai, B., Xu, X., Jia, K., Qing, C., Tao, D. (2016). DehazeNet: An end-to-end system for single image haze removal. IEEE Transactions on Image Processing, 25(11): 5187-5198. https://doi.org/10.1109/TIP.2016.2598681

[10] Wang, J.B., He, N., Zhang, L.L., Lu, K. (2015). Single image dehazing with a physical model and dark channel prior. Neurocomputing, 149: 718-728. https://doi.org/10.1109/TIP.2016.2598681

[11] Meng, G., Wang, Y., Duan, J., Xiang, S., Pan, C. (2013). Efficient image dehazing with boundary constraint and contextual regularization. In Proceedings of the IEEE International Conference on Computer Vision, pp. 617-624. https://doi.org/10.1109/ICCV.2013.82

[12] Chen, C., Do, M.N., Wang, J. (2016). Robust image and video dehazing with visual artifact suppression via gradient residual minimization. European Conference on Computer Vision, pp. 576-591. https://doi.org/10.1007/978-3-319-46475-6_36

[13] Ancuti, C., Ancuti, C.O., De Vleeschouwer, C., Bovik, A.C. (2016). Night-time dehazing by fusion. In 2016 IEEE International Conference on Image Processing (ICIP), pp. 2256-2260. https://doi.org/10.1109/ICIP.2016.7532760

[14] Zhang, J., Cao, Y., Wang, Z. (2014). Nighttime haze removal based on a new imaging model. In 2014 IEEE International Conference on Image Processing (ICIP), pp. 4557-4561. https://doi.org/10.1109/ICIP.2014.7025924

[15] Li, Y., Tan, R.T., Brown, M.S. (2015). Nighttime haze removal with glow and multiple light colors. In Proceedings of the IEEE International Conference on Computer Vision, pp. 226-234. https://doi.org/10.1109/ICCV.2015.34

[16] Yu, T., Song, K., Miao, P., Yang, G., Yang, H., Chen, C. (2019). Nighttime single image dehazing via pixel-wise alpha blending. IEEE Access, 7: 114619-114630. https://doi.org/10.1109/ACCESS.2019.2936049

[17] Sayed, M.S., Delva, J. (2010). Low complexity contrast enhancement algorithm for nighttime visual surveillance. 10th International Conference on Intelligent Systems Design and Applications, pp. 835-838. https://doi.org/10.1109/ISDA.2010.5687158

[18] Santra, S., Chanda, B. (2016). Day/night unconstrained image dehazing. 23rd International Conference on Pattern Recognition (ICPR), pp. 1406-1411. https://doi.org/10.1109/ICPR.2016.7899834

[19] Xie, B., Guo, F., Cai, Z. (2010). Improved single image dehazing using dark channel prior and multi-scale retinex. IEEE International Conference on Intelligent Systems Design and Engineering Applications (ISDEA), pp. 848-851. https://doi.org/10.1109/ISDEA.2010.141

[20] Hari, U., Bevi, A.R. (2022). Dark and bright channel priors for haze removal in day and night images. Intelligent Automation and Soft Computing, 34(2): 957-967. https://doi.org/10.1109/CVPRW.2009.5206515

[21] Ancuti, C., Ancuti, C.O., De Vleeschouwer, C., Bovik, A.C. (2020). Day and night-time dehazing by local airlight estimation. IEEE Transactions on Image Processing, 29: 6264-6275. https://doi.org/10.1109/TIP.2020.2988203

[22] Rahman, Z.U., Jobson, D.J., Woodell, G.A. (2004). Retinex processing for automatic image enhancement. Journal of Electronic Imaging, 13(1): 100-110. https://doi.org/10.1117/1.1636183

[23] Choi, D.H., Jang, I.H., Kim, M.H., Kim, N.C. (2008). Color image enhancement using single-scale retinex based on an improved image formation model. In 2008 16th European Signal Processing Conference, pp. 1-5.

[24] Guo, F., Cai, Z., Xie, B., Tang, J. (2010). Automatic image haze removal based on luminance component. In 2010 6th International Conference on Wireless Communications Networking and Mobile Computing (WiCOM), pp. 1-4. https://doi.org/10.1109/WICOM.2010.5600632

[25] Wang, J., Lu, K., Xue, J., He, N., Shao, L. (2017). Single image dehazing based on the physical model and MSRCR algorithm. IEEE Transactions on Circuits and Systems for Video Technology, 28(9): 2190-2199. https://doi.org/10.1109/TCSVT.2017.2728822

[26] Gilboa, G., Osher, S. (2007). Nonlocal linear image regularization and supervised segmentation. Multiscale Modeling & Simulation, 6(2): 595-630. https://doi.org/10.1137/060669358

[27] Buades, A., Coll, B., Morel, J.M. (2011). Non-local means denoising. Image Processing on Line, 1: 208-212. https://doi.org/10.5201/ipol.2011.bcm_nlm

[28] Hou, G., Wang, G., Pan, Z., Huang, B., Yang, H., Yu, T. (2017). Image enhancement and restoration: state of the art of variational retinex models. IAENG International Journal of Computer Science, 44(4): 445-455.

[29] Zosso, D., Tran, G., Osher, S.J. (2015). Non-local retinex---a unifying framework and beyond. SIAM Journal on Imaging Sciences, 8(2): 787-826. https://doi.org/10.1137/140972664

[30] Chung, Y.L., Chung, H.Y., Chen, Y.S. (2020). A study of single image haze removal using a novel white-patch retinex-based improved dark channel prior algorithm. Intelligent Automation and Soft Computing, 26(2): 367-383. https://doi.org/10.31209/2020.100000206

[31] Ancuti, C.O., Ancuti, C., De Vleeschouwer, C., Bekaert, P. (2017). Color balance and fusion for underwater image enhancement. IEEE Transactions on Image Processing, 27(1): 379-393. https://doi.org/10.1109/TIP.2017.2759252

[32] Li, L., Wang, R., Wang, W., Gao, W. (2015). A low-light image enhancement method for both denoising and contrast enlarging. IEEE International Conference on

Image Processing, pp. 3730-3734. https://doi.org/10.1109/ICIP.2015.7351501
[33] Al-Hashim, M.A., Al-Ameen, Z. (2020). Retinex based multiphase algorithm for low-light image enhancement. Traitement du Signal, 37(5): 733-743. https://doi.org/10.18280/ts.370505
[34] Wang, W., Wu, X., Yuan, X., Gao, Z. (2020). An experiment-based review of low-light image enhancement methods. IEEE Access, 8: 87884-87917. https://doi.org/10.1109/ACCESS.2020.2992749
[35] Park, S., Yu, S., Moon, B., Ko, S., Paik, J. (2017). Low-light image enhancement using variational optimization-based retinex model. IEEE Transactions on Consumer Electronics, 63(2): 178-184. https://doi.org/10.1109/ICCE.2017.7889233
[36] Guo, X., Li, Y., Ling, H. (2016). LIME: Low-light image enhancement via illumination map estimation. IEEE Transactions on Image Processing, 26(2): 982-993. https://doi.org/10.1109/TIP.2016.2639450
[37] Gupta, B., Agarwal, T.K. (2018). New contrast enhancement approach for dark images with non-uniform illumination. Computers & Electrical Engineering, 70: 616-630. https://doi.org/10.1016/j.compeleceng.2017.09.007
[38] Rivera, A.R., Ryu, B., Chae, O. (2012). Content-aware dark image enhancement through channel division. IEEE Transactions on Image Processing, 21(9): 3967-3980. https://doi.org/10.1109/TIP.2012.2198667
[39] He, K., Sun, J., Tang, X. (2012). Guided image filtering. IEEE Transactions on Pattern Analysis and Machine Intelligence, 35(6): 1397-1409. https://doi.org/10.1109/TPAMI.2012.213
[40] Zhu, Q., Yang, S., Heng, P. A., Li, X. (2013). An adaptive and effective single image dehazing algorithm based on dark channel prior. In 2013 IEEE International Conference on Robotics and Biomimetics (ROBIO), pp. 1796-1800. https://doi.org/10.1109/ROBIO.2013.6739728
[41] Xiao, C., Gan, J. (2012). Fast image dehazing using guided joint bilateral filter. The Visual Computer, 28(6): 713-721. https://doi.org/10.1007/s00371-012-0679-y
[42] Adams, A., Baek, J., Davis, M.A. (2010). Fast high-dimensional filtering using the permutohedral lattice. In Computer Graphics Forum, 29(2): 753-762. https://doi.org/10.1111/j.1467-8659.2009.01645.x
[43] Ancuti, C., Ancuti, C.O., De Vleeschouwer, C. (2016). D-hazy: A dataset to evaluate quantitatively dehazing algorithms. IEEE International Conference on Image Processing, pp. 2226-2230. https://doi.org/10.1109/ICIP.2016.7532754
[44] Wang, A., Wang, W., Liu, J., Gu, N. (2018). AIPNet: Image-to-image single image dehazing with atmospheric illumination prior. IEEE Transactions on Image Processing, 28(1): 381-393. https://doi.org/10.1109/TIP.2018.2868567
[45] Ren, W., Liu, S., Zhang, H., Pan, J., Cao, X., Yang, M. H. (2016). Single image dehazing via multi-scale convolutional neural networks. European Conference on Computer Vision, pp. 154-169. https://doi.org/10.1007/978-3-319-46475-6_10
[46] Kimmel, R., Elad, M., Shaked, D., Keshet, R., Sobel, I. (2003). A variational framework for retinex. International Journal of Computer Vision, 52(1): 7-23. https://doi.org/10.1023/A:1022314423998
[47] Rudin, L.I., Osher, S., Fatemi, E. (1992). Nonlinear total variation based noise removal algorithms. Physica D: Nonlinear Phenomena, 60(1-4): 259-268. http://doi.org/10.1016/0167-2789(92)90242-F